# Thermal Response and Damage Features of Fabricated Steel Structures under Fire

Lu Xia, Yingle Wei*

Anhui Vocational and Technical College of Water Conservancy and Hydropower, Hefei 231603, China

Corresponding Author Email: 17756086226@163.com

**ABSTRACT**

Figuring out the thermal response and damage features of fabricated steel structures under fire conduces to enhancing the fire resistance of steel structures and lowering the probability of fire accidents. Available methods are able to simulate complex fire situations, but their accuracy is affected by the adopted models and calculation methods. For this reason, this paper researched the thermal response and damage features of fabricated steel structures under fire. At first, the thermal response of fabricated steel structures under fire was analyzed, the ultimate bearing capacity and the fire resistance was calculated and checked. Then, the evolution of fatigue damage of fabricated steel structures under fire was analyzed, and the fatigue damage evolution method and its flow were given. At last, combining with actual cases, the thermal response and damage features of fabricated steel structures under fire were examined experimentally, and the results verified the validity of the proposed analysis method.

## 1. INTRODUCTION

Fabricated steel structures are widely used in all kinds of engineering projects these days due to their many merits including fast installation, controllable quality, and recyclable materials [1-8]. However, as an emergency event, fire accidents can greatly affect the stability and bearing capacity of steel structures, and there are a lot of blanks in the research on the thermal response and damage features of fabricated steel structures under fire [9-14]. Thus, research efforts to fill in these blanks are of utterly importance [15-18] since they could not only contribute to enhancing the fire resistance of steel structures and lowering the probability of fire accidents [19, 20], but also provide useful technical support for engineering design, construction and management, thereby promoting the application of fabricated steel structures in more projects. The attained research results could serve as both theoretical evidence and practical experience for formulating fire prevention specifications and design guidelines, ultimately dedicating to raising the fire prevention level of the entire construction industry.

Alam et al. [21] made investigations to understand the conditions under which a travelling fire may start and develop and its impact on surrounding steel structures. Authors performed the fire test for two times with normal and reduced sizes of openings to simulate different ventilation conditions, observed the behavior of traveling fire, and recorded the gas temperatures at different levels and locations. The impact of traveling fire on surrounding structure was studied based on recorded temperatures of selected steel columns and beams, and the impact of ventilation condition was discussed by comparing the results of the second fire test with the records made before the first fire test. Their study revealed that travelling fire produces non-uniform temperatures in the compartment irrespective of ventilation conditions although the magnitude of this non-uniformity is related with the size of

the opening, and such non-uniformity exists along the length as well as along the height of the test compartment. Hou et al. [22] established a regression model for researching the high temperature performance of steel strands which can be used for both theoretical analysis and numerical calculation. Based on a non-stationary temperature field model constructed for fire in tall and large space buildings, the authors adopted a non-linear finite element numerical analysis method with time integral effect taken into account to build a fire resistance numerical model for large-span pre-stressed steel structures, and used a beam structure fire-resistance calculation example to discuss the impact of different fire source positions on the fire-resistance of pre-stressed steel structures. Manco et al. [23] reported the results of a numerical investigation work aiming at assessing the structural safety of an actual offshore topside steel structure exposed to accidental localized fire conditions, and discussed the nonlinear thermo-mechanical and ultimate strength behaviors attained via two means: sophisticated CFD (Computational Fluid Dynamics) and LF-ESF (Localised Fire with Ellipsoidal Solid Flame), which were previously developed and validated by the authors. CFD-based approaches usually use the input energy given by a combustion model to solve nearly compressible flows, and make accurate evaluation on the fluid's thermal response in the entire duration of a simulated accident. However, analysis complexity, massive produced data, and long computational time make the CFD approaches unsuitable for the current design. In contrast to CFD approaches, the proposed LF-ESF approach could give accurate estimates and the modelling can be directly performed in FE-based commercial software to get the temperature changes and thermo-mechanical behaviors of the steel. Their research results indicate that the LF-ESF approach combined with FE-based models can give reliable fire-safety analyses, ensuring that the main safety (load-bearing) functions of the offshore steel structures are not impaired during accidental fire conditions.

Currently available methods for analyzing the thermal response and damage features of fabricated steel structures under fire can be divided into several types: theoretical analysis methods, experimental research methods, and finite element analysis methods. The accuracy of theoretical methods is often constrained by models and assumptions; the experimental methods cost too much, and can hardly simulate all possible fire situations due to limited test conditions; the accuracy of finite element analysis is also affected by models and calculation methods even though it can simulate complex fire situations. In view of these matters, this paper researched the thermal response and damage features of fabricated steel structures under fire. In the second chapter, the thermal response of fabricated steel structures under fire was analyzed, the ultimate bearing capacity and the fire resistance was calculated and checked. In the third chapter, the evolution of fatigue damage of fabricated steel structures under fire was analyzed, and the fatigue damage evolution method and its flow were given. At last, combining with actual cases, the thermal response and damage features of fabricated steel structures under fire were examined experimentally, and the results verified the validity of the proposed analysis method.

## 2. THERMAL RESPONSE OF FABRICATED STEEL STRUCTURE IN FIRE

Fire can cause dramatic temperature rise to steel structures, thereby reducing their strength and stiffness. The calculation of ultimate bearing capacity is helpful to evaluate the stability and safety of steel structures in case of fire, supplementing evidences for fire prevention design, and guaranteeing the safety of personnel and property. Excessive design can cause resource waste and increase project cost. By calculating the ultimate bearing capacity, reasonable section size, material grade and protective measure could be determined for steel structures, avoiding the unnecessary excessive design. Also, the evaluation of the damage degree of steel structures after fire could provide evidences for post-disaster recovery and repair works, ensuring construction quality and safety. Figure 1 shows the model for calculating the ultimate bearing capacity adopted in this paper.
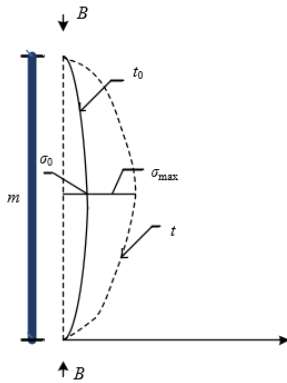


**Figure 1.** Calculation model of ultimate bearing capacity

In this study, assumptions and methods under normal temperature conditions were adopted to calculate the ultimate bearing capacity of fabricated steel structures under fire, specifically, assuming: $t_0$ represents the initial bending of a constant-pressure rod, there is:

$$t_0 = \sigma_0 \sin(\tau z/m) \tag{1}$$

The deflection curve of steel structure under axial pressure is given by the following formula:

$$t = [\sigma_0/(1 - B/B_{RY})]\sin(\tau z/m) \tag{2}$$

Assuming: $S$ represents the sectional area of the steel structure, $\eta$ represents the slenderness ratio of the steel structure, $R_Y$ represents the elastic modulus of the member at high temperature, then the Euler critical force of the fabricated steel structure under axial pressure at high temperature can be calculated as follows:

$$B_{RY} = \delta_{RY} S \tag{3}$$

$$\delta_{RY} = \tau^2 R_Y / \eta^2 \tag{4}$$

If the maximum deflection of the steel structure appears at the m/2 position, then the maximum deflection can be calculated by the following formula:

$$\sigma_{MA} = t\big|_{z=m/2} = \sigma_0/(1 - B/B_{RY}) \tag{5}$$

At the center point position, the cross section of the steel structure is subjected to axial pressure $B$ and the bending moment, satisfying $L = B\sigma_{MA}$; if the resistance bending moment of the cross section is represented by $Q$, then the formula for calculating the edge stress of the section is:

$$\delta = B\delta_{max} \Big/ Q + \frac{B}{S} \tag{6}$$

Assuming: $r_0 = \sigma_0 S/Q$ represents the initial eccentric distance of the steel structure, by combining Formulas 5 and 6, we have:

$$\delta = \frac{B}{S}\left[\frac{\sigma_0/S}{1 - B/(S\delta_{RY})} + 1\right] \tag{7}$$

The following formula gives the ultimate stress state of the steel structure:

$$\sigma_{XHY}\left(\frac{r_0}{1 - \delta_{XHY}/\delta_{RY}} + 1\right) = d_{tY} \tag{8}$$

The critical stress of axially compressed rods of steel structure under fire can be calculated by the following formula:

$$\delta_{XHY} = \left\{ \begin{array}{l} (1 + r_0)\delta_{RY} + d_{tY} \\ -\sqrt{\left[(1 + r_0)\delta_{RY} + d_{tY}\right]^2 - 4d_{tY}\delta_{RY}} \end{array} \right\} \Big/ 2 \tag{9}$$

The critical stress of axially compressed rods of steel structure at room temperature can be calculated by the following formula:

$$\delta_{XHY} = \left\{ \begin{array}{l} (1 + r_0)\delta_R + d_t \\ -\sqrt{\left[(1 + r_0)\delta_R + d_t\right]^2 - 4d_t\delta_Y} \end{array} \right\} \Big/ 2 \tag{10}$$

Fire resistance check calculation is a key link to evaluate the safety performance of steel structures under fire, it can check whether a steel structure can maintain a stable bearing capacity under fire within a specified duration or not, thereby ensuring the safety of personnel and property. Fire resistance check calculation is a statutory requirement during building design and construction processes. According to the construction codes of each country and region, building structures must meet requirements for a certain fire resistance level to make sure that when a fire starts, they could buy enough time for personnel evacuation and fire rescue. Through fire resistance check calculation, people can discover potential risks with steel structures under fire conditions, thereby making optimizations to the fire protection design. The results of fire resistance check calculation can help engineers understand the performance changes of steel structures under fire, laying a basis for assessing the structural damage at fire, making reasonable arrangement of post-disaster recovery and repair works, and assuring good construction quality and safety.

If the type parameter of the cross section is represented by $\varepsilon$, then according to the calculation of ultimate bearing capacity, $\delta_{XHY}$ and $\delta_{XH}$ can be expressed by Formulas 11 and 12. Assuming: $\theta_Y$ represents the stability coefficient of the fabricated steel structure under axial pressure at high temperature, $\theta$ represents the stability coefficient of the fabricated steel structure under axial pressure at room temperature, then there are:

$$\delta_{XHY} = \theta_Y d_{tY} \tag{11}$$

$$\delta_{XH} = \theta d_t \tag{12}$$

$$\theta_Y = \beta_v \theta \tag{13}$$

where, $\beta_v = 1 + \eta s_1 \eta^3$, $0 \leq \eta \leq 80$; $\beta_v = 1 + \eta s_2 \{1 - 3.29 \times 10^{-6}(250 - \eta)^{2.4}\}$, $80 \leq \eta \leq 250$. In this paper, after attaining $\theta_Y$ and $\delta_{XH}$, the fire resistance check calculation was performed further. Assuming: $d_{tY}$ represents the yield strength of steel at high temperature, $\varepsilon_E$ represents the resistance coefficient of steel, $d_Y$ represents the design strength of steel at high temperature, then there is:

$$\frac{B}{\theta_Y S} \leq d_{tY} \tag{14}$$

Assuming: $B$ represents the design value of the fabricated steel structure under axial pressure during fire, $S$ represents the gross section area of the axially compressed rod, that is $\theta_Y = \beta_v \theta$, $\beta_v$ represents the stable check calculation parameter of the fabricated steel structure under axial pressure at high temperature, then the formula above can be written in another form:

$$\frac{B}{\theta_Y S} \leq \varepsilon_E d \tag{15}$$

## 3. FATIGUE DAMAGE EVOLUTION OF FABRICATED STEEL STRUCTURE UNDER FIRE

Analysis of the fatigue damage evolution of fabricated steel structures under fire involves the relationship between the thermodynamic state variables and the damage variables of the

steel structure. Under fire conditions, the thermodynamic state variables of steel structure include temperature, stress, strain, etc., and the damage variables mainly reflect the damage degree and failure risk of the structure. There is a certain relationship between the two types of variables. During fire disasters, the temperature rise of steel structures is the main cause of structural damage, as the temperature increases, both the strength and stiffness of the steel decline significantly, thereby leading to a drop in the bearing capacity of the structure. In the meantime, temperature rise can also cause thermal expansion and a large thermal stress, which can further aggravate structural damage. Figure 2 shows the temperature measuring points of a common steel structure subjected to fire on four sides. Under fire conditions, stresses acted on the steel structure mainly include thermal stress and mechanical stress. The thermal stress originates from thermal expansion caused by temperature gradient, while the mechanical stress comes from factors such as the weight and load of the structure. Stress increment can accelerate the development of structural damage, causing expansion of fatigue cracks, in severer cases, structural failure. Under fire conditions, the strain of steel structures contains thermal strain and mechanical strain. Similarly, thermal strain is caused by thermal expansion, and mechanical strain is related to stress. The increase of strain can cause the structure to deform and reduce its bearing capacity and service life. When the strain exceeds the strain tolerance of steel, the structure will face the risk of failure.
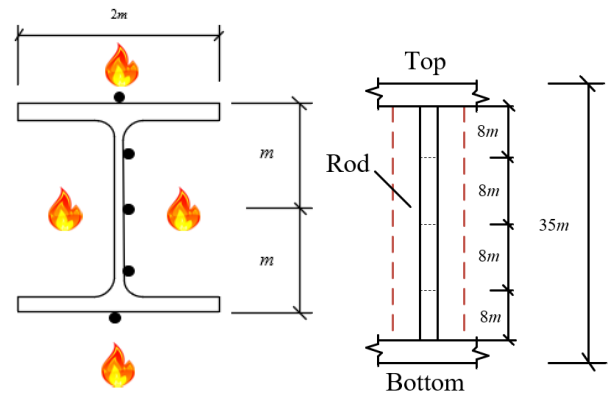


**Figure 2.** Measuring points of a steel structure with four sides on fire

In the analysis of fatigue damage evolution of fabricated steel structures under fire, the constitutive relationship of basic units of damage and fracture involves the response of steel structure under different thermodynamic conditions. The basic unit constitutive relationships are mathematical models that describe the correlations between stress, strain, and damage of materials under different states. The basic unit constitutive model adopted in this study is the *Lemaitre* damage model, which uses a damage variable to measure the damage degree $F$ of materials based on the concepts of equivalent stress and equivalent strain. In this model, damage variable $D$ increases with stress and strain, when damage degree $F$ reaches the critical value, the material will break.

Based on the known *Lemaitre* damage model, the fatigue damage of steel structure under fire can be assessed by considering the monotonic stress-strain curve in a single fatigue loading cycle and the law of damage evolution. In a single cycle of fatigue loading, at first, the monotonic stress-

strain curve needs to be determined, which describes the stress-strain relationship experienced by the steel structure during a single loading. In this loading process, stress increment can cause minor damages, and the accumulation of these minor damages conforms to the law of damage evolution, which is given by the basic unit constitutive model. In the unloading stage, since the unloading process does not produce additional damage, there's no need to take into account its effect on the damage. By taking the range-variant integral of the loading stress, the cumulative damage increment in a single cycle of fatigue loading can be calculated, which can represent the damage degree of the steel structure in one fatigue cycle.
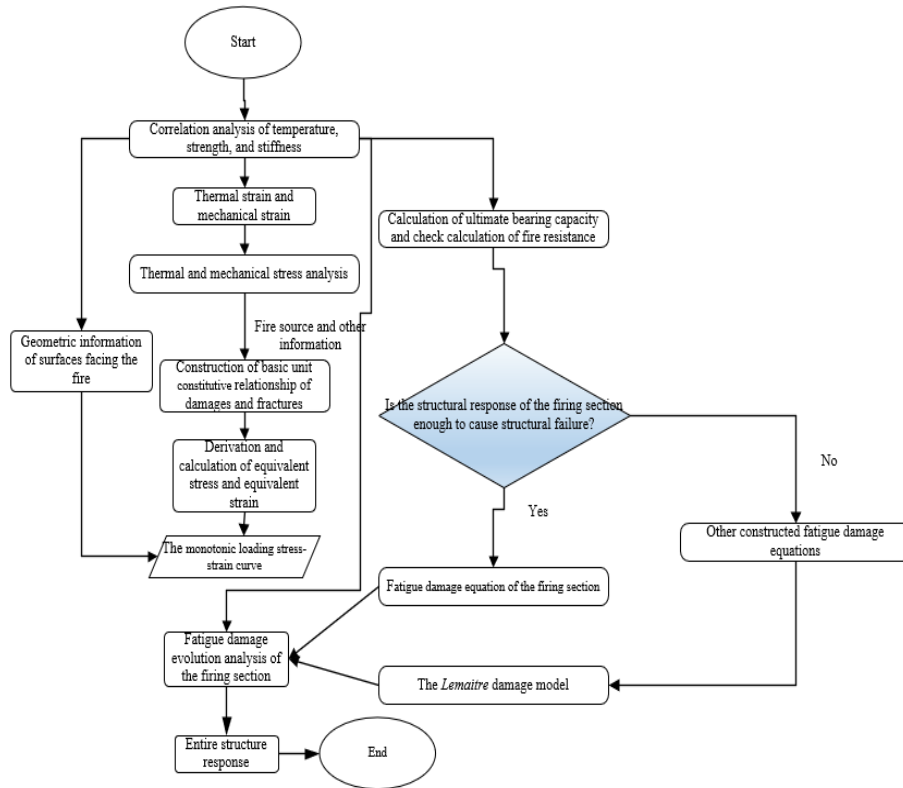


**Figure 3.** Methods and flow of fatigue damage evolution analysis

The specific derivation process of the above flow is detailed below. Figure 3 gives the methods and flow of fatigue damage evolution analysis. At first, the release rate of damage strain energy was introduced into the constitutive damage evolution law of basic units under the condition of stress increment, then there is:

$$F = \left(\frac{\tilde{\delta}^2}{2Rs}\right)^b \tau = \left(\frac{\delta^2}{2Rs(1-F)^2}\right)^n \tau \tag{16}$$

Assuming: $j$ represents the material constant, then the power function relationship existing between micro plastic strain and effective stress by assumption can be expressed as:

$$\tau = \left(\frac{\tilde{\delta}^2}{j}\right)^l = \left(\frac{\delta}{j(1-F)}\right)^l \tag{17}$$

Taking the differentials of the above formula, there is:

$$\tau = l\left(\frac{\delta}{j(1-F)}\right)^{l-1}\frac{1}{j}\tilde{\delta} \tag{18}$$

To characterize the coupling effect between stress and damage during the loading process of fabricated steel

structures under fire, the following formula is given:

$$\tilde{\delta} = \frac{\delta}{1-F} + \frac{\delta F}{(1-F)^2} \tag{19}$$

Above analysis shows that the variation of effective stress consists of two parts: one part is caused by changes in actual nominal stress, and the other part is caused by changes in damage. Changes in effective stress can affect the damage evolution process of the steel structure, let $m=2n+1$ and $X=(1/2Rs)^n l/j^l$, and further combine Formulas 19, 18 with 16 to get:

$$F = \frac{X\delta^{m-1}(1-F)\delta}{(1-F)^{m+1} - X\delta^m} \tag{20}$$

By performing circulatory integration on above formula, we can get:

$$\frac{\sigma F}{\sigma B} = \int_{\delta_{MI}}^{\delta_{MA}} \frac{X\delta^{m-1}(1-F)}{(1-F)^{m+1} - X\delta^m} f\delta \tag{21}$$

Because the fatigue damage evolution equation of steel structures shown in Formula 20 is non-linear, the stress and damage of steel structure are not independent by default, so the explicit expression of $\sigma F/\sigma B$ cannot be derived from above

formula. To solve this matter, this paper introduced a normalized damage variable, let $F\rightarrow\infty$, then there is:

$$(1-F)^{m+1} = X\delta^m \tag{22}$$

The residual strength $\delta_e$ can be calculated by the following formula:

$$\delta_e(F) = \left(\frac{(1-F)^{m+1}}{X}\right)^{\frac{1}{m}} \tag{23}$$

When $F$ is equal to 0, the steel structure has no fatigue damage, and the ultimate strength $\delta_a$ of the steel structure is:

$$\delta_a = \left(\frac{1}{x}\right)^{\frac{1}{m}} \tag{24}$$

Above two formulas were combined to get:

$$\delta_e = \delta_a(1-F)^{\frac{m+1}{m}} \tag{25}$$

When the residual strength of the steel structure reaches the fatigue loading stress level $\delta_{MA}$, the structure is in a critical state of fatigue damage, and the damage at this time is the critical damage. Figure 4 shows the critical fatigue damage and deformation of steel structures. The formula for calculating the critical damage value is:

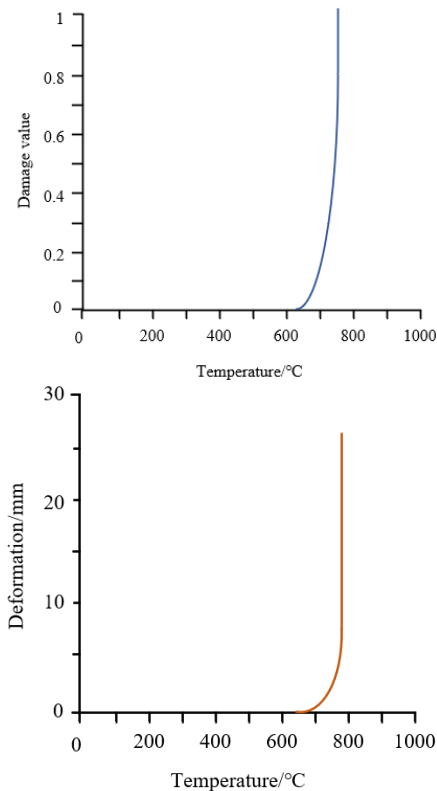$$F_v = 1 - \left(X\delta^m\right)^{\frac{1}{m+1}} \tag{26}$$



**Figure 4.** Critical fatigue damage and deformation of steel structure

In simple words, the normalized damage variable can simplify the nonlinear damage evolution equation, making the evolution processes of damage variables defined by various macroscopic physical quantities consistent and can be easily applied to engineering projects. During analysis, the damage variable can be defined as micro datum (such as micro cracks or voids) or as macro datum (such as stress or strain). Although the damage variables defined by macroscopic physical quantities are local, they can reflect the relationship between damage threshold and loading level under various definitions and directly show the evolution law of fatigue damage. So in actual engineering application cases, defining normalized damage variables can simplify the damage evolution equation and make the variables defined by different macroscopic physical quantities have similar evolution processes, thereby facilitating comparison and analysis. At the same time, the normalized damage variable can transform damage phenomenon of different scales into a uniform dimension, which is convenient for the study of damage mechanism and engineering applications. Assuming: $F_v(\delta_{MA})$ represents the critical damage value under definitions of various physical quantities, $F_v(\delta_{MA})$ represents the macroscopic damage variable, then the generalized damage variable $FB$ can be expressed as:

$$F_B = \frac{F(\delta_{MA})}{F_v(\delta_{MI})}; (0 \le F \le F_v, 0 \le F_B \le 1) \tag{27}$$

Assuming: $m(.)=m(n,l,F_v(A_{MA}),A_{MA})$ represents a scalar function, so dimensionless maximum loading stress ratio $A_{MA}=\delta_{MA}/\delta_a$ was adopted. $L(.)=L(R,s,n,j,l,F_v(\delta_{MA}),\delta_{MA})$. After introducing $F_B$, Formula 21 can be simplified:

$$\frac{\partial F_B}{\partial B} = \int_{\delta_{MI}}^{\delta_{MA}} \frac{\delta^{m(.)}}{L(.)(1-F_B)^{m(.)+1}} f\delta \tag{28}$$

When $F=F_v$, there must be $F\rightarrow\infty$.

Formally speaking, the variable in Formula 28 is separable, but in fact, $F_B$ and $\delta$ are not independent, so the explicit expression of $\sigma F/\sigma B$ cannot be derived from the above formula, and the formula needs to be simplified further. The integral result of above formula contains the exponential term of loading stress amplitude $\Delta\delta=\delta_{MA}-\delta_{MI}$ and the exponential term of $1-F_B$. $\sigma F_B/\sigma B$ is a scalar, so the result of above formula can be expressed by a dimensionless variable function. Similarly, transform $\delta$ and $L(.)$ into dimensionless form, then the integral result contains the ratio of range-variate strain, and the exponential term is 3 dimensionless variables $A_{MA}=\delta_{MA}/\delta$, $A_{MI}=\delta_{MI}/\delta$, and $F_v(A_{MA})$. $b(A_{MA},A_{MI},F_v(A_{MA}))$ was introduced into the exponential term of $(1-F_B)$ to represent the correlation between $A_{MA}$, $A_{MI}$, and $F_v(A_{MA})$. To figure out the impact of average stress ratio $A_l=A_{MA}-A_{MI}/2$ on the fatigue life of steel structure, a scalar function $L_b(A_l,F_v(A_{MA}))$ related to the material composition of steel structure was introduced. Assuming: $A_{XY}$ represents the equivalent stress, $L(A_l,F_v)$ and $b(A_{MA},A_{MI},F_v)$ are related to temperature and material of the steel structure, based on above analysis, Formula 28 can be simplified to the explicit expression shown below:

$$\frac{dF_B}{dB} = \left\{\frac{A_{XY}}{L(A_l,F_v)(1-F_B)}\right\}^{b(A_{MA},A_{MI},F_v)} \tag{29}$$

Assuming: $B_{XH}$ represents the number of cycles in the beginning of the damage of fabricated steel structure under fire, $B_d$ represents the number of cycles when the structure starts to crack, by integrating above formula and letting $F=0$ when $B=B_{XH}$ and $F=1$ when $B=B_d$, we can get:

$$\frac{dF_B}{dB} = \left\{ \frac{A_{XY}}{L(A_l,F_v)(1-F_B)} \right\}^{b(A_{MA},A_{MI},F_v)} \tag{30}$$

$$-\frac{(1-F_B)^{b(A_{MA},A_{MI},F_v)+1}}{b(A_{MA},A_{MI},F_v)+1} + \frac{1}{b(A_{MA},A_{MI},F_v)+1}$$

$$= \left[ \frac{A_{XY}}{L(A_l,F_v)} \right]^{b(A_{MA},A_{MI},F_v)} (B-B_{XH}) \tag{31}$$

$$B_d = B_{XH}$$

$$+\frac{1}{b(A_{MA},A_{MI},F_v)+1}\left[ \frac{A_{XY}}{L(S_l,f_v)} \right]^{-b(A_{MA},A_{MI},F_v)} \tag{32}$$

By combining above two formulas, the final fatigue damage evolution equation of fabricated steel structures under fire can be attained as:

$$F_B = 1 - \left( 1 - \frac{\dfrac{B}{B_d} - \dfrac{B_{XH}}{B_d}}{1 - \dfrac{B_{XH}}{B_d}} \right)^{\frac{1}{b(A_{MA},A_{MI},F_v)+1}} \tag{33}$$

where, $B_d$, $B_{XH}$, and $b(A_{MA},A_{MI},F_v)$ are determined by the experiment.

## 4. EXPERIMENTAL RESULTS AND ANALYSIS

Table 1 shows the temperature of different sections of the steel structure during stable stage under fixed scenarios. Based on the data in above table, the temperature values of different sections of the steel structure during stable stage in fixed scenarios could be analyzed.

**Table 1.** Temperature of different sections of steel structure during the stable stage in fixed scenarios

| 2m | Stabilized temperature of the second temperature rise/°C | The final stabilized temperature/°C | 8m | The final stabilized temperature/°C |
|---|---|---|---|---|
| 1 | 559 | 500 | 1 | 530 |
| 2 | 499 | 430 | 2 | 260 |
| 3 | 359 | 330 | 3 | 282 |
| 4 | 1045 | 1200 | 4 | 931 |
| 5 | 498 | 432 | 5 | 446 |
| 6 | 364 | 352 | 6 | 323 |
| 7 | 503 | 431 | 7 | 495 |
| 8 | 452 | 387 | 8 | 295 |
| 9 | 352 | 333 | 9 | 270 |

**Table 2.** Damage values of measuring points of steel structure at different temperatures

| Temperature/°C | 20 | 100 | 200 | 300 | 400 | 500 | 600 | 700 | 800 |
|---|---|---|---|---|---|---|---|---|---|
| Deformation | 0.0324 | 0.0345 | 0.0366 | 0.0432 | 0.0556 | 0.08 | 0.0856 | 1.8531 | 23.504 |
| Damage | 0 | 1.32E-06 | 0.0002 | 0.0005 | 0.0009 | 0.0016 | 0.0021 | 0.0759 | 1 |

First, it is noted that, at each measuring point, the final stabilized temperature values are generally lower than the stabilized temperature values of the second temperature rise, indicating that as the fire develops, the heat will gradually spread to the surroundings, lowering local temperature of the steel structure, and this phenomenon may be related to the gradual weakening of fire source or the depletion of combustion materials. Second, at 2m and 8m heights, the trends of the final stabilized temperature are not the same. According to the data, with the increase of the serial number of measuring points, at 2m height, the final stabilized temperature fluctuates, at 8m height, the final stabilized temperature shows an obvious decline trend, indicating that during the fire, in high temperature areas, the temperature curve changes slower, this might because the hot air rises during fire, and accumulates at the ceiling gradually.

Above analysis suggests that, during fire, as the height increases, for the temperature of different sections of the steel structure during the stable stage, the curve curvature of measuring points at higher positions is gentler, this conclusion reflects the slow accumulation process of hot air at the roof, and this is helpful for understanding the influence of fire on the steel structure.

Table 2 shows the damage values of steel structure measuring points at different temperatures. Based on the table data, the damage of these measuring points at different temperatures can be analyzed. Judging from the perspective of the trend of damage value, as the temperature rises, damage value shows a dramatic increase. During low temperature stage (20-300°C), the damage value is smaller, but when the temperature exceeds 400°C, the damage value grows rapidly, indicating a significant increase in the damage of the steel structure at high temperature conditions. Increment of damage value means that the strength and stiffness of the steel structure both decrease, which can result in an increase in the overall deformation of the node area, an increase in the deflection of mid-span, and changes in the thermal additional internal force. As the damage value increases, the overall deformation of the steel structure increases significantly. At high temperatures, the strength and stiffness of the steel structure decline, leading

to an obvious overall deformation in the node area. The increase of damage value also causes significant changes in the deflection of the mid-span of the steel structure. As the temperature rises, the stiffness of the steel structure decreases, which can increase the deflection of the mid-span, thereby affecting the stability and safety of the building. Moreover, the increase of damage value can complicate the trend of thermal additional internal force. At high temperatures, the strength and stiffness of the steel structure decrease, making the thermal additional internal force distribute unevenly, thus affecting the stability of the structure.
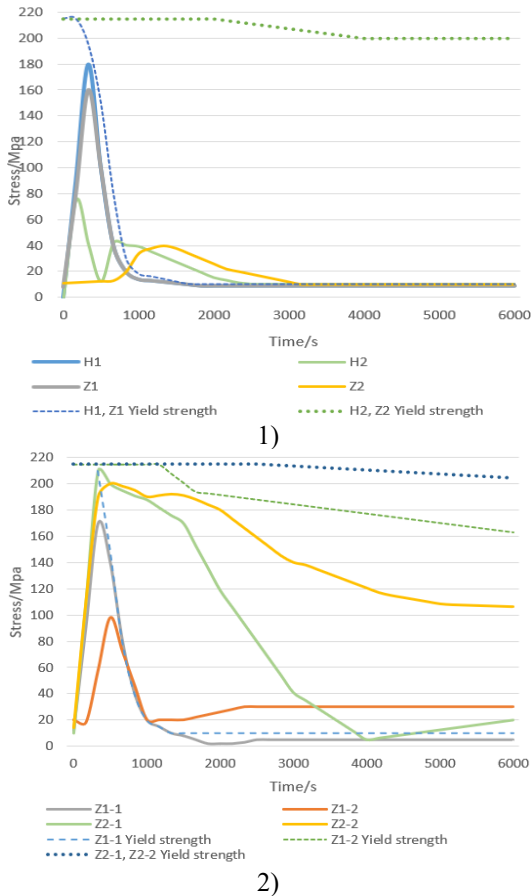


1)



2)

**Figure 5.** Time-stress curves of key measuring points at the bottom plate of the steel structure

Figure 5 shows the time-stress curves of key measuring points at the bottom plate of the steel structure. Based on these curves, the time-stress variations of key measuring points at the bottom plate of the steel structure can be analyzed. First, by observing the stress changes at measuring points $H1$ and $Z1$, we can see that their stress values increase fast in the early stage, and decrease slowly after reaching the peak. In contrast, at measuring points $H2$ and $Z2$, the stress values increase slowly in the early stage, and gradually tend to be stable after a certain period of time. In terms of yield strength, the yield strength of $H1$ and $Z1$ decreases gradually with the passing of time, and the yield strength of $H2$ and $Z2$ remains stable basically. This indicates that although $H1$ and $Z1$ were subjected to a greater stress, this might lead to local yield of the steel structure; $H1$ and $Z1$ were subjected to a smaller stress, in these areas, the safety of the steel structure is higher. The stress value of measuring point $Z1$-1 rises rapidly during the early stage and gradually decreases after reaching the peak, indicating possible yield in this area under stress; then over

time, the yield strength of $Z1$-1 gradually decreases, which further verifies a low safety level of this area. The stress value of measuring point $Z1$-2 rises slowly during the early stage, then after a certain time, it gradually approaches stable. The stress at $Z1$-1 and $Z1$-2 rises fast in the early stage, and tends to be stable after reaching the peak. In these areas, the yield strength remained stable, indicating a higher safety level. To ensure a higher overall safety of the bottom plate of the steel structure, attentions should be paid to the stress variation at $Z1$-1 and its yield strength decline, corresponding measures could be taken for reinforcement or the design could be optimized. In the meantime, attentions on stress stability of $Z1$-2, $Z2$-1, and $Z2$-2 are also required to ensure the safety of the entire steel structure at different times.
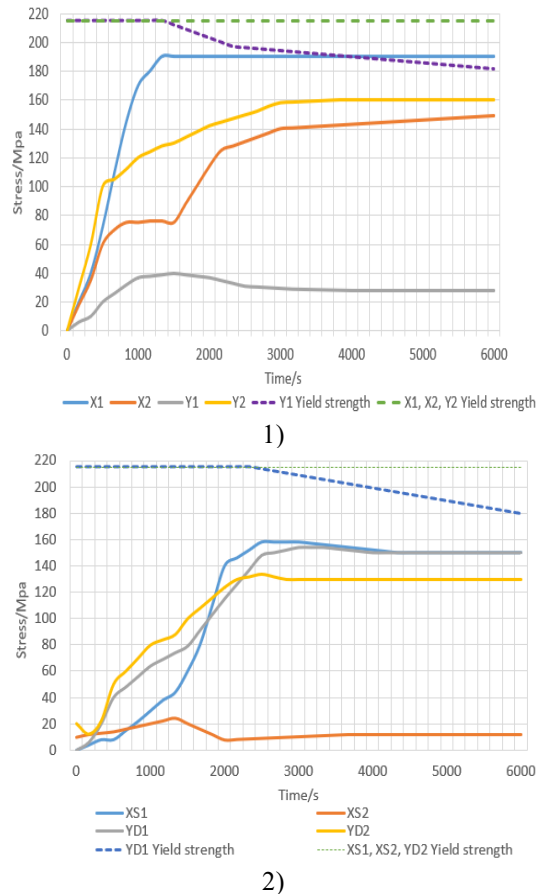


1)



2)

**Figure 6.** Time-stress curves of key measuring points at corners and edges of the steel structure

Figure 6 shows the time-stress curves of key measuring points at corners and edges of the steel structure. By analyzing data in the two graphs we can know the stress variations at different times and the reaching of yield strength. Observations of stress changes at measuring points X1 and X2 show that, stress at the two points rises rapidly in the early stage, and tends to be stable after reaching the peak. In contrast, the stress values of measuring points Y1 and Y2 exhibit different trends, stress at Y1 grows slowly in the early stage and tends to be stable after reaching the peak; while the stress at Y2 grows rapidly in the early stage and remains at a high level after reaching the peak. In terms of yield strength, it can be seen that the yield strength of Y1 decreases over time, while the yield strength of X1, X2 and Y2 remains stable basically, indicating that Y1 was subjected to a large stress, which might cause local yield of the steel structure; the stress at other

measuring points was smaller, indicating a higher safety in these areas. In the meantime, the stress value of measuring point YD1 grows rapidly in early stage, and tends to be stable after reaching the peak, indicating that the yield phenomenon may appear in these areas under stress. As the time passes, the yield strength of YD1 decreases gradually, which further verifies a low safety level in these areas. The stress values of measuring points XS1 and XS2 vary slightly, indicating a higher safety level in these areas. The stress value of measuring point YD2 fluctuates greatly, but overall speaking, it shows an upward trend, and the yield strength in this area remains stable, also indicating a higher safety level. In order to ensure the overall safety of measuring points at corners and edges of the steel structure, attentions should be paid to stress variation at YD1 and the decline of yield strength, also, corresponding measures could be taken for reinforcement or the design could be optimized. In addition, attentions on the stress stability of XS1, XS2 and YD2 are required to ensure the safety of the entire steel structure at different times.
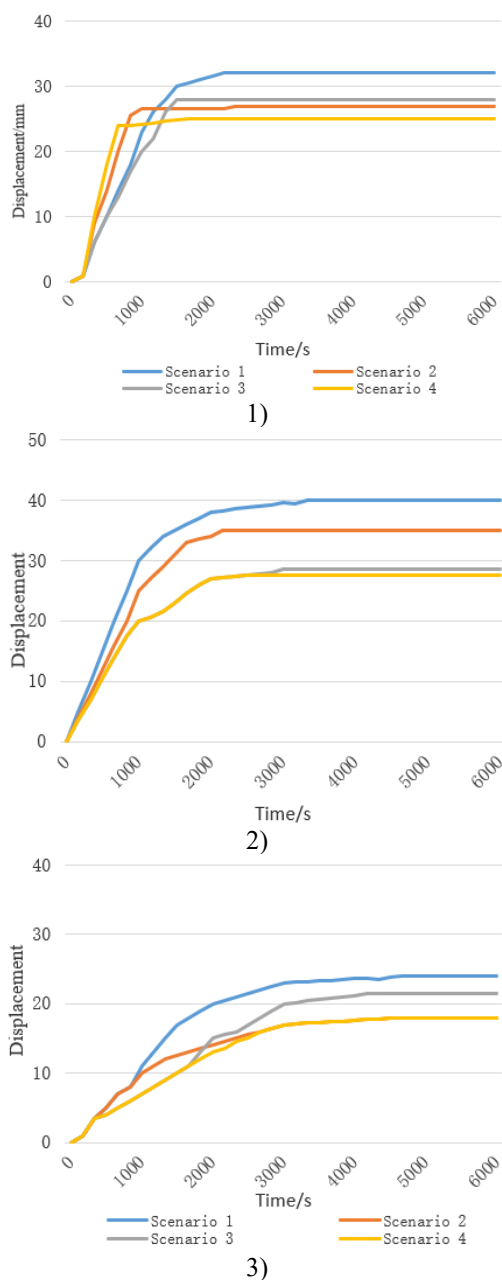


1)



2)



3)

**Figure 7.** Comparison of maximum displacement of steel structure measuring points in different fire scenarios

Figure 7 compares the maximum displacement of steel structure measuring points in different fire scenarios. According to the figure, for most measuring points at different times, the stress doesn't exceed the yield strength. In terms of X direction displacement, in Scenarios 2 and 4, the X direction displacement is larger, indicating in these fire scenarios, the steel structure may undergo a greater deformation in the X direction, so attentions need to be paid to fire prevention measures and structural design. In terms of Y direction displacement, in Scenarios 1 and 2, the Y direction displacement is larger, indicating in these fire scenarios, the deformation of the steel structure in Y direction is more obvious, corresponding fire prevention measures and structural design are required to ensure the safety of the building. In terms of Z direction displacement, in Scenario 1, displacement in Z direction is the largest, indicating significant deformation of the steel structure in this direction, and it might need stricter fire prevention measures and structural design to ensure the safety of the building; in Scenarios 2, 3, and 4, the displacement in Z direction is smaller, but attentions are still required for fire prevention measures and structural design. To sum up, in different fire scenarios, the stress and displacement at different measuring points of the steel structure vary in different directions. These factors need to be comprehensively considered during design and construction phases, and appropriate fire prevention measures and structural design should be adopted to ensure the safety of the building. In addition, during operation, changes in the stress and displacement at key measuring points should be closely monitored to ensure the long-term safety of the building.

## 5. CONCLUSION

This paper researched the thermal response and damage features of fabricated steel structures under fire. At first, the thermal response of fabricated steel structures under fire was analyzed, the ultimate bearing capacity and the fire resistance was calculated and checked. Then, the evolution of fatigue damage of fabricated steel structures under fire was analyzed, and the fatigue damage evolution method and its flow were given. Combining with actual cases, the thermal response and damage features of fabricated steel structures under fire were examined experimentally, and the results verified the validity of the proposed analysis method. In the experimental part, the temperature values of different sections of the steel structure under fixed scenarios were given; the damage values of steel structure measuring points at different temperatures were given and analyzed; the time-stress curves of key measuring points at bottom plate, corners, and edges of the steel structure were plotted and analyzed; and the maximum displacement of steel structure measuring points in different fire scenarios was compared. At last, this paper proposed a few countermeasures for the discovered matters, including comprehensively considering factors during design and construction, taking appropriate fire prevention measures and structural design to ensure the safety of the building, and paying close attention to stress and displacement changes at key measuring points to ensure long-term safety of the building.

## REFERENCES

[1]  Shi, S. (2021). Research on the application mode of

prefabricated steel structure building design based on BIM technology. Journal of Physics: Conference Series, 1992(2): 022052. https://doi.org/10.1088/1742-6596/1992/2/022052

[2] Qiao, C., Pan, Q., Zhang, Z., Hu, P. (2019). Research on component recycling based on steel structure prefabricated building. IOP Conference Series: Earth and Environmental Science, 330(2): 022079. https://doi.org/10.1088/1755-1315/330/2/022079

[3] Qiao, C., Hu, P., Pan, Q., Geng, J. (2019). Research on $CO_2$ emission reduction of a steel structure prefabricated building considering resource recovery. IOP Conference Series: Earth and Environmental Science, 237(2): 022036. https://doi.org/10.1088/1755-1315/237/2/022036

[4] Shi, Y., Zhou, X.H., Liu, L.P. (2019). Shaking table test on prefabricated light steel structure popular science building. Journal of Building Structures, 40(2): 98-107.

[5] Gao, L. (2019). Pit-retaining structure construction technique of h-shaped steel anchor composite pile-prefabricated wallboard adopting compaction grouting method of a high-rise building in Guangzhou. IOP Conference Series: Earth and Environmental Science, 295(4): 042086. https://doi.org/10.1088/1755-1315/295/4/042086

[6] Hao, J.P., Sun, X.L., Xue, Q., Fan, C. L. (2017). Research and applications of prefabricated steel structure building systems. Engineering Mechanics, 34(1): 1-13. https://doi.org/10.6052/j.issn.1000-4750.2016.08.ST14

[7] Liu, J., Liu, Q., Feng, Y. (2019). Structural behavior of self-drilling screws applied in steel structures of prefabricated buildings. IOP Conference Series: Earth and Environmental Science, 267(5): 052030. https://doi.org/10.1088/1755-1315/267/5/052030

[8] Loss, C., Piazza, M., Zandonini, R. (2016). Connections for steel-timber hybrid prefabricated buildings. Part I: Experimental tests. Construction and Building Materials, 122: 781-795. https://doi.org/10.1016/j.conbuildmat.2015.12.002

[9] Lu, L.M., Yuan, G.L., Shu, Q.J., Li, Q.T. (2018). Numerical analysis on the fire behavior of a steel truss structure. In Life Cycle Analysis and Assessment in Civil Engineering: Towards an Integrated Vision, CRC Press, pp. 2033-2038.

[10] Suwondo, R., Cunningham, L., Gillie, M., Bailey, C. (2021). Analysis of the robustness of a steel frame structure with composite floors subject to multiple fire scenarios. Advances in Structural Engineering, 24(10): 2076-2089. https://doi.org/10.1177/1369433221992494

[11] Behnam, B., Abolghasemi, S. (2021). Post-earthquake fire performance of a generic fireproofed steel moment resisting structure. Journal of Earthquake Engineering, 25(13): 2579-2604. https://doi.org/10.1080/13632469.2019.1628128

[12] Liu, J., Wu, X., Li, H., Cai, Y. (2019). Study on water based ultra-thin fire resistive coating for steel structure and the fire resistance test. IOP Conference Series: Earth and Environmental Science, 218(1): 012074.

https://doi.org/10.1088/1755-1315/218/1/012074

[13] Shi, J., Yang, Y.Q. (2019). Study on base resin of fire-proof and anticorrosive steel structure coatings. IOP Conference Series: Materials Science and Engineering, 542(1): 012064. https://doi.org/10.1088/1757-899X/542/1/012064

[14] Charlier, M., Glorieux, A., Dai, X., Alam, N., Welch, S., Anderson, J., Vassart, O., Nadjai, A. (2021). Travelling fire experiments in steel-framed structure: numerical investigations with CFD and FEM. Journal of Structural Fire Engineering, 12(3): 309-327. https://doi.org/10.1108/JSFE-11-2020-0034

[15] Ye, J., Chen, W. (2021). Experimental study on fire resistance of full-scale cold-formed steel composite shear wall structure under real fire conditions. Jianzhu Jiegou Xuebao/Journal of Building Structures, 42(6): 59-71.

[16] Zhan, W., Chen, L., Gu, Z., Jiang, J. (2020). Influence of graphene on fire protection of intumescent fire retardant coating for steel structure. Energy Reports, 6: 693-697. https://doi.org/10.1016/j.egyr.2019.11.139

[17] Ambroziak, A., Piotrkowski, P., Heizig, T. (2019). Assessment of technical condition and repair of steel structure elements on the example of fire damage in a warehouse building. In MATEC Web of Conferences, 284: 02001. https://doi.org/10.1051/matecconf/201928402001

[18] Shao, S., Jia, G., Cao, L., Deng, G. (2019). Research on post-fire metallographic structure and hardness of quenched and tempered high strength steel 07MnMoVR. In Pressure Vessels and Piping Conference, 58943: V003T03A060. https://doi.org/10.1115/PVP2019-93423

[19] Wei, F., Zheng, Z., Yu, J., Wang, Y. (2019). Structure behavior of concrete filled double-steel-plate composite walls under fire. Advances in Structural Engineering, 22(8): 1895-1908. https://doi.org/10.1177/1369433218825238

[20] Kloos, M., Walls, R.S. (2019). Finite element modelling of the structural behaviour of a novel cellular beam non-composite steel structure in fire. International Journal of Steel Structures, 19(5): 1367-1380. https://doi.org/10.1007/s13296-019-00215-5

[21] Alam, N., Nadjai, A., Charlier, M., Vassart, O., Welch, S., Sjöström, J., Dai, X. (2022). Large scale travelling fire tests with open ventilation conditions and their effect on the surrounding steel structure–the second fire test. Journal of Constructional Steel Research, 188: 107032. https://doi.org/10.1016/j.jcsr.2021.107032

[22] Hou, J., Li, H., Xie, D., Qian, L., Tang, B. (2022). Fire resistance analysis of prestressed steel structure based on the study of high temperature mechanical properties of steel strands. In Advances in Transdisciplinary Engineering, Springer, pp. 990-995. https://doi.org/10.1007/978-3-030-85223-9_84

[23] Manco, M.R., Vaz, M.A., Cyrino, J.C., Landesmann, A. (2021). Thermomechanical performance of offshore topside steel structure exposed to localised fire conditions. Marine Structures, 76: 102924. https://doi.org/10.1016/j.marstruc.2020.102924